Volume 1 | Number 1 | Jan 2013 | Pages 1–100

Dalton Transactions

An international journal of inorganic chemistry
www.rsc.org/dalton

ROYAL SOCIETY OF CHEMISTRY

ROYAL SOCIETY OF CHEMISTRY

www.rsc.org/dalton

Dalton Transactions

ARTICLE

Helix–Coil Transition Induced by Metal Ion Interaction with a Grafted Iron–Binding Site of the CyaY Protein Family

Diego S. Vazquez[a,‡], William A. Agudelo[a,‡], Angel Yone[a], Nora Vizioli[a], Martín Arán[b], F. Luis González Flecha[a], Mariano C. González Lebrero[a,*] and Javier Santos[a,*]

Iron–protein interactions are involved in electron transfer reactions. Alterations of these processes are present in a number of human pathologies; among then, in Friedreich's ataxia, in which a deficiency in functional frataxin, an iron–binding protein, leads to the progressive neuromuscular degenerative disease. The putative iron–binding motif of acidic residues EExxED was selected from the first α–helical stretch of the frataxin protein family and grafted on a foreign peptide scaffold corresponding to the C–terminal α–helix from *E. coli* thioredoxin. The resultant grafted peptide named GRAP was studied applying experimental (circular dichroism, isothermal titration calorimetry, capillary zone electrophoresis, thermal denaturation, NMR) and computational approaches (docking, molecular dynamics simulations). Although isolated GRAP lacks a stable secondary structure in solution, when iron is added, the peptide acquires an α–helical structure. Here we have shown that the designed peptide is able to specifically bind Fe^{3+} with moderate affinity (K_D= 1.9±0.2 μM) and a 1:1 stoichiometry. Remarkably, GRAP/Fe^{3+} interaction is entropically driven ($\Delta H°$=-1.53 ± 0.03 kcal mol^{-1} and T$\Delta S°$ =6.26 kcal mol^{-1}). Experiments and simulations indicate that Fe^{3+} interacts with the peptide through three acidic side chains, inducing the α–helical conformation of the grafted motif. In addition, the acidic side chains involved undergo significant conformational rearrangements upon binding, as judged by the analysis of MDs. Altogether, these results contribute to an understanding of the iron–binding mechanisms in proteins and, in particular, in the case of human frataxin

Introduction

Iron is an essential element for living cells. Iron–protein interactions are involved in electron transfer reactions, vital for a large number of physiological processes. Alterations of these processes are present in aceruloplasminemia, as well as in Hallervorden–Spatz syndrome, Parkinson and Huntington diseases, and Friedreich's ataxia, among other human pathologies.[1-6]

Mammalian frataxin (FXN) is a small (14.3kDa) nuclear–encoded mitochondrial protein.[7-11] It has been shown that FXN binds both metal ions, Fe^{2+} and Fe^{3+}, working as an iron chaperone.[12] This protein plays an essential role in the regulation of the iron–sulfur (Fe–S) cluster biosynthesis intervening in iron donation to the Fe–S cluster machinery and in the fine regulation of cysteine desulfurase, a crucial activity for cluster assembly.[8, 13, 14] In addition, FXN takes part in heme synthesis through direct interaction with ferrochelatase, the enzyme that inserts iron into protoporphyrin IX to form heme.[15]

A deficiency in functional FXN in humans leads to the progressive neuromuscular degenerative disease Friedreich's ataxia, which affects children and adolescents with an estimated incidence of 2 to 3 out of 100,000 births.[16] Most patients (95% of cases) carry a GAA triplet repeat expansion in the first intron on both alleles of the gene–encoding FXN protein, whereas 5% of cases show a point mutation in one allele in combination with GAA expansion in the second.[2, 16, 17]

Some aspects of iron–FXN interaction have already been studied. It is well known that FXN coordinates iron atoms through exposed glutamate and aspartate side chains located in α1, loop1 and β1 secondary structure elements (the acidic ridge of FXN), on the protein surface.[10, 18] However, the affinity and the mechanism for interaction between the metal ion and the protein are not completely understood, one of the difficulties

being the existence of multiple–binding sites on the FXN surface, varying among homologs.[19] Pastore *et al.* found out that FXN from *E. coli* exhibits relatively low cation specificity and contains multiple metal–binding sites, which are able to chelate divalent and trivalent cations with low or moderate affinity.[20] In addition, FXN iron–binding capacity seems to be quite robust. Correia *et al.* have shown that even when five of the most conserved acidic residues from the putative iron-binding region of yeast FXN were mutated to Ala, at least two iron atoms per monomer were able to be bound, although with a weakened affinity. Because these FXN mutants gain thermodynamic stability upon mutation, the authors have concluded that the acidic ridge has evolved favouring function over protein stability.[21]

The evident complexity of the iron–binding process results in the impossibility of evaluating the K_D value for each metal-binding site, and consequently, an average K_D was estimated from measurements. In this context, the examination of the properties of a consensus iron-binding site emerges as crucial step to understanding FXN–mediated processes.

Our strategy in studying iron-protein interaction consists of grafting a putative iron-binding motif of acidic residues on a foreign peptide scaffold. The binding motif was selected from the first α–helical stretch of the FXN protein family (CyaY in PFAM), and the well–studied C–terminal amphipathic peptide (TRXP) from *E. coli* thioredoxin (EcTRX)[22, 23] was used as the scaffold. TRXP in solution, whether or not in the presence of iron, does not exhibit spectroscopic signatures compatible with a periodic secondary structure, whereas in the context of EcTRX this peptide adopts a stable α–helical conformation. On the other hand, the tendency of isolated TRXP to acquire secondary structure is increased by the presence of inductors like TFE or SDS, and strongly depends on residues located in the apolar face of the peptide that can establish i-i+4 interactions.[23, 24] In this context, we hypothesised that iron binding to the putative motif grafted on the peptide would induce α–helical conformation of the peptide. This strategy resorts to a simple model–system to study the iron–binding process in which the free peptide and peptide/iron complex formation would exhibit clear–cut distinctive experimental signals.

In this paper, the resultant grafted peptide (GRAP) was studied, applying experimental and computational approaches, and iron–peptide interaction and its consequences on peptide conformation and molecular dynamics were explored.

Results and discussion, Experimental

Grafting of an Iron–binding Motif of Acidic Residues

Analysis of the X–ray structure of metal–FXN complexes[20], multiple sequence alignment (MSA) of FXN protein sequences, information provided by metal titration of ^{15}N–FXN from *E. coli* followed by NMR[19], and biochemical and mutational information from FXN variants[25] has enabled us to postulate a consensus for an iron–binding motif of acidic residues. A number of acidic residues conserved throughout evolution were detected and a series of possible iron–binding sites came into view, most of them located in the context of the helix α1, loop1 and strand β1 elements (**Figure 1**).
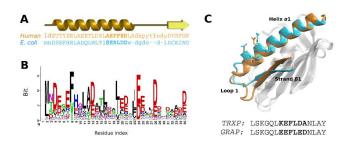

Figure 1. Searching for Iron–binding Motifs in the Acidic Ridge of FXN. (A) Alignment of the acidic ridge region (helix α1, loop 1 and strand β1) of human and *E. coli* FXN sequences. (B) Sequence LOGO of the CyaY family. (C) Ribbon diagram of human and *E. coli* FXN structures, showing the acidic ridge region (orange and cyan, respectively). Acidic side chains of the motif are in sticks. The sequences of peptides TRXP and GRAP are shown, and the region involved in the motif grafting is in bold. Molecular graphics were prepared using VMD.[26]

In this work, we have studied a putative binding site of sequence EExxED, which is a mixture of sequences located in α1 helix (**Figure 1**) found in human (EExxD, ExxED and EDxxD), *Psychromonas ingrahamii* (EExxEE) and *Escherichia coli* (EExxDD) FXN variants, and which is represented in the MSA by the EExxED sequence found in the *Candida albicans* homolog. In addition, we have investigated the characteristics of the side chains located in–between the acidic residues (xx residues). Evidence provided by bioinformatics indicates that the first intercalated x position may be occupied by residues of wide–range physicochemical properties (e.g., charged, uncharged, polar, apolar, **Figure S1A**). This position does not seem to be conserved and frequently is partially accessible to the solvent. On the other hand, an apolar residue, Leu, Ile, Phe or Val, (in this order of preference) usually is located in the second x position (**Figure S1B**). Each position may contribute to the stability of the protein establishing local interactions (for instance intra–α–helical i-i+4 contacts that increase the tendency to form a helical structure, in agreement with AGADIR[27] results, Figures S1 C and D), and tertiary contacts with the rest of the protein (FOLDX[28, 29] results for human, *E. coli* and *P. ingrahamii* variants, **Figure S2** and Supplementary Information).

This evidence suggests a structural role for at least one of the central xx residues in the helical context providing the protein with stability; mutation is in general predicted to destabilize. On the other hand, acidic residues located in the α1 helix destabilize the protein whereas mutation is predicted to stabilize (FOLDX results **Figure S2** and Correia *et al.*[21]). These positions are, in general, energetically frustrated and they are conserved or partially conserved through evolution for protein function.

In this context, our working hypothesis is that acidic residues have the main functional role of the motif, whereas the central xx side chains mostly contribute to the structural stability of the scaffold. Taking into account the above, and given the physicochemical characteristics of the central xx residues, we decided to maintain the sequence of TRXP for these positions (residues Phe–Leu). It is noteworthy that in TRX peptide these residues increase the amphipathicity and the tendency to form α–helical structure by establishing local interactions as judged by previous results of our laboratory.[23]

Experimental Characterization of Grafting: Iron Binding, Specificity and Conformation

When the EExxED pattern of acidic residues was grafted, the tendency of the new peptide (GRAP) to form a stable α–helical structure in the presence of the inductor SDS diminished by comparison with TRXP, more likely due to the presence of the negative acidic side–chain cluster (**Figure S3A**). Accordingly, the addition of 50 mM NaCl to the 2.5 mM SDS/GRAP solutions enhanced α-helical content (**Figure S3B**). Moreover, the addition of 25 % v/v TFE promoted the transition to α-helical conformations of both peptides (**Figure S3C**). These results indicate that like TRXP, the grafted peptide is able to acquire a periodic structure in solution under certain experimental conditions.

In this context, we evaluated whether metal ions could promote the coil–to–helix transition, a fact that can be interpreted as strong evidence of binding. **Figure 2A** shows the changes in the far-UV CD spectra observed after the addition of Fe^{3+} to the GRAP and TRXP samples. The presence of metal ion in GRAP solutions determines an enhancement of far–UV CD signals at 208 and 222 nm, compatible with an increment in the α–helical content of 5–6 residues, as judged by ellipticity. Remarkably, more than 50 % of the CD signal remains unaltered after heating the sample and equilibration up to 70 °C (**Figure 2B**). In the same fashion, Fe^{2+}, in the presence of the reducing agent 1.0 mM TCEP, produces significant increments of the CD signals, compatible with metal binding and stabilization of the secondary structure (**Figure 3**), in agreement with results previously obtained for FXN protein.[30] Interestingly, Al^{3+} also determines secondary structure stabilization. On the other hand, neither Ca^{2+}, Cd^{2+}, Co^{2+}, Cu^{2+}, Mg^{2+}, Mn^{2+}, Zn^{2+} nor Ni^{2+} substantially promote structure acquisition (**Figure 3**). Remarkably, GRAP is also able to interact with Pd^{2+}. In this case, however, the complex shows a far–UV CD spectrum compatible with stabilization of the β-structure (**Figure S4**).

Our results demonstrate that GRAP has a certain specificity for Fe^{2+} and Fe^{3+}. To avoid problems related to the redox properties of iron, we decided to work with Fe^{3+} at pH 4.1, a condition in which iron is soluble. Moreover, in this condition, chemical modification of GRAP is minimized, making the understanding of the peptide/metal interaction mechanism simpler.

Figure 3. Specificity of the Metal–Binding Site. The induction of the GRAP α–helical secondary structure upon the metal ions addition was followed by the CD signal at 222 nm. The cations were incubated at 25 °C with 20 μM GRAP in 20 mM Tris–HCl buffer, pH 7.0 or 5 mM potassium acetate, pH 4.1. The metal ions Ca^{2+}, Cd^{2+}, Co^{2+}, Cu^{2+}, Mg^{2+}, Mn^{2+}, Zn^{2+} or Ni^{2+} were in 10:1 and Fe^{2+}, Fe^{3+}, and Al^{3+} in 3:1 molar ratio (metal to peptide).

To evaluate possible changes in the aggregation state of the peptide GRAP upon metal binding, we carried out pulse field gradient NMR self–diffusion measurements experiments[31, 32] and the effective hydrodynamic radius (R_h) was measured in the absence or in the presence of Fe^{3+}. The measured R_h for GRAP (9.5±0.3Å), obtained by using dioxane as an internal standard at pH 4.1, perfectly agrees with the R_h measured for TRXP (10.0±0.2Å [22, 24]). More importantly, there was no increase in R_h upon metal supplementation (R_h=7.7±1.1Å), strongly suggesting that the GRAP/Fe^{3+} complex behaves as a monomer, even suffering a slight compaction upon metal binding, in accordance with a partial induction of α–helix observed by CD, without significant tendency to aggregate in these experimental conditions (**Figure 4 A**). Furthermore, the analysis of 1D ^{1}H–NMR spectra indicates that iron directly interacts with the peptide because incubation with the paramagnetic metal ion Fe^{3+} (3:1 molar ratio) results in the extinction of signal peaks from amide regions and changes in ^{1}H chemical shifts (**Figure 4B**).

As the net charge of GRAP changed after Fe^{3+} binding, we used capillary zone electrophoresis (CZE) to detect the complex formation. It is worthy of note that when peptide and Fe^{3+} were pre–incubated before CZE, the mobility of the peptide changes according to the expected change in charge (**Figure S5**).

To evaluate the affinity of the interaction between iron and GRAP, we performed titrations of the peptide with FeCl$_3$ at 25 °C. Titrations were followed both by ITC (**Figures 5A and B**) and by far–UV CD spectroscopy (**Figure 5C**).
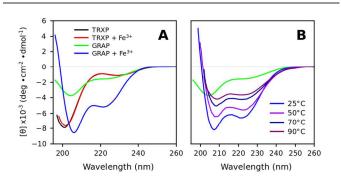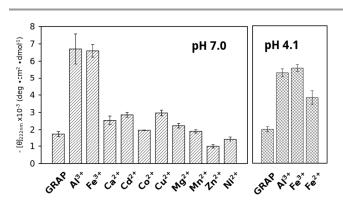

Figure 2. Induction of α-helical Conformation by Fe^{3+}. (A) Far-UV CD spectra corresponding to GRAP in the absence (green) or in the presence (blue) of a 5–fold excess of the metal ion are shown. Spectra of TRXP in the presence or in the absence of iron (black and red, respectively) are also shown. (B) GRAP Far–UV CD spectra in the presence of a 5–fold excess of iron at different temperatures (25, 50, 70 to 90 °C). As a reference, GRAP in the absence of Fe^{3+} is shown in green. Buffer was 5.0 mM potassium acetate pH 4. Peptide concentration was 30 μM.
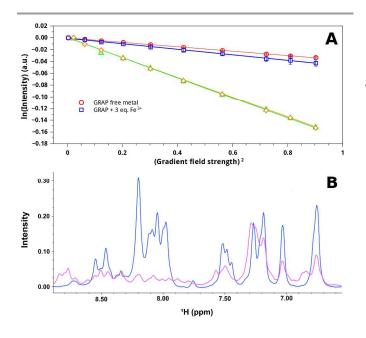
Figure 4. Diffusion Curves by NMR. (A) GRAP was incubated at 25 °C with or without Fe^{3+} in a 3:1 molar ratio (metal to peptide). Diffusion measurements were carried out using the PFG–SLED sequence using a calibration constant of 53.5 G/cm. Dioxane was added to each peptide sample (with (Δ) or without ($\Diamond$) iron) as an internal standard. For representation, each curve was normalized by the corresponding diffusion time Δ(d20). (B) ^{1}H–NMR spectra obtained in the presence or in the absence of Fe^{3+} are shown. Buffer was 5 mM potassium acetate, pH 4.1.

The use of 20 mM potassium acetate, pH 4.1, aimed to increase the solubility of iron and avoid precipitation of the metal buffer. Titration by ITC yielded $n= 0.90 \pm 0.01$, $K = (5.4 \pm 0.5) \times 10^5$ M^{-1}, $\Delta H° = -1.53 \pm 0.03$ kcal mol^{-1} and $T\Delta S° = 6.26$ kcal mol^{-1}. In agreement with these results, titrations followed by CD at 222 nm, performed at three different concentrations of peptide (20, 30 and 40 µM) yielded an affinity constant of $K= (2.2 \pm 1.7) \times 10^6$ M^{-1}. On the other hand, spectroscopic (**Figure 2A**) and calorimetric signals corresponding to TRXP solutions do not show any appreciable change upon the addition of iron (data not shown).

Computational Characterization of Grafting: Geometry, Side Chain and Backbone Conformations

We performed computational simulations to evaluate the molecular details leading to iron binding. First, we parametrized the Fe^{3+} ion in water using thermodynamic integration on MDs (**Table S1 and Figure S6**). Then, conformational searches were carried out in combination with docking of the metal ion (see Supplementary Information for details). Only bi– and tridentate geometries were obtained. The lowest free energy structures, two different tridentate complexes (**Table S2**), were studied: *complex 1,* where GRAP directly interacts with iron via E7, E8 and E11, and *complex 2,* interacting via E8, E11 and D12 (**Figures 6D, 6F and S7**). Interestingly, we have not observed tetradentate geometries in the α-helical context for complexes peptide-Fe^{3+}; this is more likely the consequence of the long distance that separates the

fourth acidic side chain from the metal ion. Similar results were obtained for isolated TRXP (**Figure S8**), in agreement with previous results by our laboratory using a Gromos force field.[23, 24]

Figure 5. Titration of GRAP with Fe^{3+}. (A) ITC traces and (B) binding isotherms after subtraction of the heat of iron dilution. (C) Fe^{3+} titration of GRAP followed by CD at 222 nm. The solid line in B and C corresponds to nonlinear regression fittings of the binding model to the data. Titrations were carried out at 25 °C in 20 mM potassium acetate, pH 4.1. Peptide concentration in (C) was 20, 30 and 40 µM. In this case, the fitting was performed using common n and K values for the three CD data sets.

Therefore, computational evidence suggests that the acidic motif may interact with Fe^{3+}, thus forming stable complexes in two alternative ways: using EExxE or through ExxED acidic residues. This result is consistent with the presence of both alternative patterns in protein sequences of diverse FXN variants. Although the EExxED motif contains two alternative binding sites, the motif may interact only with one Fe^{3+}, in accordance with ITC and CD titration.

The analysis of backbone–restricted (α–helical conformations) MDs shows a significant change in the distribution of side–chain rotameric populations in the presence of Fe^{3+} (**Figure S7** and **Table S3**). Residues E7, E8 and E11 in *complex 1,* as well as residues E8, E11 and D12 in *complex 2,* exhibit remarkable changes in the distribution of rotamers (**Figure S7,** left and central panels), whereas residues D12 in *complex 1* and E7 in *complex 2,* which are not directly involved in metal coordination (**Figure S7** lower left panel and top central panel, respectively), do not show any differences in their distribution by comparison with the corresponding free–metal peptide (**Figure S7**, right panels). This behaviour points to the reorientation of the acidic side chains as a consequence of metal interaction.

We have observed that in the particular case of residue D12, the X_I–t rotamer is the most present in the unbounded peptide, but for *complex 2,* in which this residue participates directly in Fe^{3+} binding, the X_I–m rotamer is required. This suggests a change in the rotameric population for this residue upon iron binding. However, results from Lovell *et al.*[33] have indicated that the X_I–m rotamer for aspartic residue is mostly populated in the PDB database for the alpha helical context. We do not rule out a certain inaccuracy of the force field used in this paper, to sample the correct rotameric population of aspartic amino acid, and in particular, D12 side–chain dynamics. This particular problem was discussed by Lindorff–Larsen *et al.*[34]

To explore in detail the conformation of peptide–iron complexes, we ran MD simulations releasing the backbone atom restraints. The hydrodynamic radii calculated from snapshots (one snap per ns for each simulation) using HYDROPRO[35] (11.7±0.5, 11.4±0.4 and 11.6±0.4 Å for metal–free GRAP, *complex 1* and *complex 2*, respectively) is in general agreement with our results obtained from the NMR experiments (9.5±0.3, and 7.7±1.1Å for metal–free GRAP and complex, respectively) and this evidence as a whole is only compatible with the monomeric state of the peptide both in isolation and in complex. Despite the loss of structure in the N– and C–terminal stretches of GRAP, the residues involved in the iron–binding motif (encompassing 5–7 residues) remained structured throughout the simulations, as judged by the analysis of Φ and Ψ torsional angles (**Figure 6**). Residues [L6, **E7**, **E8**, F9, L10, **E11**, and D12] and [**E8**, F9, L10, **E11**, and **D12**] are in an α–helical conformation in *complexes 1 and 2,* respectively (**Figures 6C**, **6F**, and **S9**). This result is in agreement with our CD experiments, demonstrating that Fe^{3+} stabilizes the α–helical structure of the iron–binding motif grafted on GRAP. On the contrary, in the absence of iron, GRAP completely loses its secondary structure in the first nanoseconds of the simulations and does not recover its starting conformation (**Figures 6A** and **D**).

The characterization of Fe^{3+}: GRAP structures using docking and MDs that we carried out showed no significant differences by comparison with results obtained from MDs of Mg^{2+}:GRAP complex (data not shown). Noteworthy, these simulations do not allow the study of the exchange of the metal ion due to the slow rate of the process (μs timescale).

In addition, we performed thermodynamic integrations for Fe^{2+}, Mg^{2+}, Co^{2+}, Mn^{2+} and Ca^{2+} metal ions (implemented in Amber14) using parameter obtained by Duarte et al.[36] **Table S5** contains a summary of these results suggesting that there is an energy gap between the binding of Fe^{2+} to GRAP and the other metal ions. However, solvation energies of the metal ions determined by TI, which represent for us a quality control, are not coincident with the experimental values, even when the radial distribution functions (metal: oxygen) are coincident with the expected ones. Thus, in this case, there is no guaranty that parameters, which correctly reproduce solvation geometries (and solvation energies in the best scenario), describe the energetics of metal:peptide interactions. To study the bases of the specificity of the motif, in terms of the energetics of the system and coordination geometries, we will use QM/MM MDS techniques in future simulations.

Discussion

Iron Binding in the Context of a Short Peptide

In this paper, we have shown that the designed peptide GRAP is able to bind Fe^{3+} with substantial affinity (K_D=1.9±0.2 μM) and a stoichiometry of 1:1, in a monomeric state. Moreover, simulations and experiments both suggest that iron interacts with the peptide through three acidic side chains, inducing the α–helical structure of a 5-6 amino acid residue stretch. This means that the EExxED acidic motif defines by itself an iron–binding site.

To validate the model structures of the complexes, the distribution of χ1 and χ2 for Glu and Asp were compared with the rotamer database of Lovell *et al.*[33] This analysis shows that rotamer populations in the simulations fall in the high probability region of the conformational space (**Table S3**). This indicates that the binding structures are possible without ligand stress.
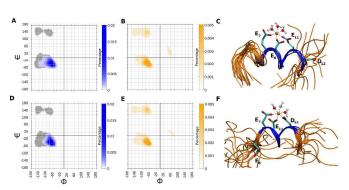
Figure 6. Analysis of Φ and Ψ Angles for Metal–peptide Complexes. For *complex 1*, residues L6, E7, E8, F9, L10, E11, and D12 are shown in (A) and residues L1, S2, K3, G4, Q5, N13, L14 and A15 are shown in (B). For *complex 2*, residues E8, F9, L10, E11, and D12 are shown in (D) and residues L1, S2, K3, G4, Q5, L6, E7, N13, L14, and A15 are shown in (E). A snapshot superimposition of the last 100 ns of MDs corresponding to *complex 1* or *complex 2* is shown in (C) and (F), respectively, using blue and orange colors for residues adopting a helical and non–helical structure, respectively. As a reference, Φ and Ψ angles for the unrestrained peptide without metal are shown in a gray color in panels (A) and (D).

Acidic side chains of GRAP undergo significant conformational rearrangements, as judged by the large changes in rotameric distributions, confirming that the acidic side chain–based iron–binding site is rather flexible, even in the context of an α–helical conformation with a restrained backbone structure. These kinds of rearrangements are common in binding sites. Gaudreault *et al.*[37] have shown that most (~90 %) ligand–binding pockets contain, at least, one side chain undergoing rotamer conformational changes, when *apo* and *holo* forms of proteins are compared. This suggests that flexibility may control some aspects of the binding process.

One question that arises from our results is why this metal–binding motif is relatively specific for iron. The 3+ charge of the metal ion may be the main factor in binding. This is supported by the interaction observed in the case of Al^{3+}. On the other hand, Fe^{2+} (unlike Ca^{2+} and Mg^{2+}) is able to interact with the acidic pattern in a similar way as Fe^{3+} does, stabilizing the helical conformation of the motif, thus indicating that other factors contribute to the process (e.g., hydration energy, coordination chemistry). In this context, the electronic distributions of the metal and the ligands, their polarizing abilities, the metal coordination number, coordination geometry and metal ligand-metal distances are all critical features that determine the structure and reactivity of the metal complex and play central roles in metal discrimination and specificity in proteins.[38]

The substitution of a *native* metal ion with a foreign one can result in conformational rearrangements of the metalloprotein. In this fashion, studies by Predki PF *et al.*[39, 40] have shown that Cd^{2+} and Co^{2+} are able to replace the native Zn^{2+} (from a Zn-finger motif, however, neither Cu^{2+} nor Ni^{2+} can maintain the complex conformation required for the DNA-binding function suggesting that square-planar geometries common for these metals in this case may result in a distortion of the complex structure that normally is defined by a tetrahedral metal site.

In the case of GRAP, the conformational plasticity of the peptide backbone and acidic side-chains can contribute to modulating the binding process. Nevertheless, iron binding, which determines an octahedral geometry of the metal site, completely favours the helical conformation. On the other hand, Pd^{2+} (as in the case of Ni^{2+} and Cu^{2+}) determines square-planar geometries. While, we have no evidences of Ni^{2+} and Cu^{2+} binding to GRAP, Pd^{2+} binds to the peptide stabilizing β–structure, an entirely different conformation of the GRAP ligand. More experiments will be performed to evaluate whether the β–structure is a consequence of a metal–induced aggregation process, in which peptide aggregates keep soluble.

On the other hand, Al^{3+} (as in the case of Fe^{3+} and Fe^{2+}) favours octahedral coordination geometries, enabling binding/folding and stabilization of the α–helical conformation of GRAP. Overall, these results suggest that the binding geometry provided by each metal is critical in the process and it is one of the determinants for binding/folding specificity. Nevertheless, we do not exclude the possibility that Ni^{2+}, Cu^{2+}, Co^{2+}, Zn^{2+}, Cd^{2+}, Mn^{2+} or Mg^{2+} might interact with the acidic residues stabilizing complexes with random-coil-like conformations, similar to the observed for free GRAP, hampering the induction of the α–helical structure. More experiments will be carried out to evaluate this point, in particular, QM/MM-based MDs may contribute to the understanding of the bases of the specificity determinants.

Despite the simplicity of the process under consideration (binding of Fe^{3+} leading to the folding of a 5-6 residue stretch of GRAP), the thermodynamics of the system may enclose some complexity. ITC results indicate that binding enthalpy is small and show that the main driving force for the binding process is the change in entropy. In addition, more than 50% of the α–helical content of the complex survives after heating and equilibration at 70 °C (**Figure 2B**), suggesting that the dissociation constant might not depend largely on temperature. However, at this moment, we have no information about the ΔC_P associated to this process and consequently we could determine the exact magnitude of this dependence. As the peptide loses conformational freedom during complex formation, contributions associated to solvent molecules, which are expelled from the surface of the peptide and iron solvation spheres to the bulk, turn the entropic change positive.

Iron Binding in the Context of Frataxin and other Proteins

The presence of acidic side chains on the surface of FXN (**Figure 1**) have been previously associated with its iron–binding capability.[10] In the case of human FXN, the number of glutamic and aspartic residues located in the N–terminal stretch of the protein is strikingly higher: 8/25 in the α1 helix, 3/9 in loop1 and 1/5 in the β1 strand. A multifaceted picture with qualitatively different metal-binding sites seems to be present on the surface of FXN. Consecutive residues may form some of them, like the motif studied in this work and those identified by analysis of X–ray structures of europium or cobalt complexes

with FXN from *E. coli* (eFXN).[20] In addition, it has been reported that His 86 from the N–terminus of human FXN may also mediate high-affinity iron interactions and is required for Fe−S synthesis by the iron–sulfur cluster assembly enzyme.[13]

This intricate array of putative metal–binding sites may be linked to particular features of FXN functionality, local stability, and dynamics. In this context, protein–protein interactions, as the ones required for S–Fe cluster assembly machine activation, might depend on the number of metal ions involved and their distribution on the surface of the complex. As the interaction between FXN and the complex occurs through contacts between the acidic ridge of FXN and positive residues of cysteine desulfurase, binding of iron to FXN will completely alter electrostatics, enabling regulation and control phenomena.[41-44] Furthermore, fine–tuning metal ion affinity by protein sequence may modulate both the functionality of each site and the crosstalk between sites.

As we have mentioned above, the K_D value measured in this work (noteworthy that for GRAP, binding and folding processes are coupled) is slightly lower than the one previously measured for the full–length human FXN (12 and 55 µM for Fe^{3+} and Fe^{2+}, respectively in buffer 100 mM HEPES, pH 7.5, and 50 mM NaCl).[30] In the case of human FXN, however, the value corresponds to an average K_D that includes ~ 4–7 binding sites. Moreover, binding of Fe^{2+} to FXN from *E. coli* under anaerobic conditions is an exothermic reaction, well described by two independent binding sites with a K_D ~ 4 µM. Nevertheless, ultrafiltration experiments indicate that there are additionally much weaker Fe^{2+} binding sites on CyaY. Interestingly, their ITC results indicate that interaction between Fe^{2+} and FXN from *E. Coli* is largely entropically driven.[45]

Remarkably, the interaction between Fe and acidic side chains of proteins has been described for other protein families, among them, Amyloid–β Alzheimer's Peptide,[46] *Candida albicans* high–affinity iron permease CaFtr1p,[47, 48] human H-chain ferritin[49] the octameric protein HbpS from *Streptomyces reticuli*[50] and the α–helical–rich keratin.[51] In the latter cases, iron binding was an entropically driven process that, more likely, is guided by changes in hydration, as shown for our minimalist model (GRAP), and also in the case of the FXN from *E. coli* [45], as mentioned above. In this context, we hope our work will help to understand relations between the structure, dynamics and activity of iron–binding proteins where interaction is mediated by glutamic and aspartic amino acid residues.

Conclusions

The EExxED motif of acidic residues, selected from the first α–helical stretch of frataxin, is able to specifically bind iron with moderate affinity and a 1:1 stoichiometry when grafted onto a foreign peptide. Iron binding induces the α–helical conformation of the grafted motif, the interaction is entropically driven, and the acidic side chains involved undergo conformational rearrangements upon binding. In all, these results contribute to the understanding of iron-binding

mechanisms in proteins and, in particular, in the case of human frataxin.

Materials and Methods

Peptide Purification

The GRAP peptide of sequence LSKGQLEEFLEDNLAY was synthesized and partially purified by GenScript Corp (Piscataway, NJ). Purification was completed by HPLC (Rainin Dynamax, NY) using a reverse phase C18 semi–preparative column (Vydac) equilibrated in 0.05% aqueous TFA. Fractions containing > 98.0% pure peptide were pooled and lyophilized. The molecular mass of GRAP (MW theoretical value: 1869 Da) was checked after HPLC by MALDI-MS. As a control sample, we prepared TRXP peptide of sequence LSKGQLKEFLDANLAY (MW theoretical value: 1810 Da), corresponding to the amphipathic C-terminal α-helix of EcTRX. A C-terminal Tyr tag was added to each peptide sequence to allow concentration. Peptide concentration was calculated by measuring absorbance in the near–UV region using a JASCO UV-550 spectrophotometer. The extinction coefficient was $\varepsilon_{280nm} = 1490$ M^{-1} cm^{-1} for both peptides. Mass spectra were acquired with a 4800 MALDI TOF/TOF plus spectrometer. Iron concentration was determined using the method of 1,10– phenanthroline [52].

Bioinformatics and Multiple Sequence Alignment

A total of 550 non–redundant frataxin sequences were obtained from a BLASTp search, using the *E. coli* frataxin sequence as query (NCBI Reference Sequence WP001115168.1), and aligned by MUSCLE using the BLOSUM62 matrix. Logo was plotted using a WebLogo online server.[53] The stability of the α–helical structure given a sequence was predicted using AGADIR.[27] The contribution of a given residue to the global stability of the protein was calculated by *in silico* mutation using FOLDX.[28, 29]

Circular Dichroism Spectroscopy

The induction of an α–helical structure by SDS, 2,2,2–trifluoroethanol (TFE), or metal ions was followed by CD signal at 222 nm using a JASCO–810 spectropolarimeter. Samples were thermostatized by a peltier thermostat controller at 25 °C. Peptides (4–30 µM final concentration) were prepared in a 20 mM Tris–HCl buffer, pH 7.0 or in a 20 mM potassium acetate buffer, pH 4.1. Buffer concentrations were maintained as low as possible to gain buffer transparency, avoiding increments in the voltage and loss of spectra quality. In addition, the pH of the samples was verified and no significant pH changes were observed after mixing.

Isothermal Titration Calorimetry

To characterize the binding process from a thermodynamic point of view, several titrations were conducted using a MicroCal VP–ITC calorimeter. ITC measurements were performed at 25 °C. Twenty injections of 15.0 µl each (480 µM of $FeCl_3$ in a 20 mM potassium acetate buffer, pH 4.1) were

done on 30.0 μM of each peptide located in the calorimeter sample cell. The first injection in each experiment was not taken into account for the fittings and analysis. The heat of ligand dilution in the buffer was subtracted from titration data. Raw data were integrated with Origin 7.0 (MicroCal).

Capillary Zone Electrophoresis

All runs were performed in a P/ACE MDQ capillary electrophoresis system (Beckman–Coulter) in an uncoated fused silica capillary (32 cm x 50 μm ID), and a UV detector was set at 214 nm for monitoring backbone signal, applying a constant voltage of 10 kV and setting capillary temperature at 25 °C. Buffer conditions were 5.0 mM potassium acetate, pH 4.1.

Determination of Hydrodynamic Radii

NMR experiments were performed at 25°C in a Bruker 600 MHz Avance III spectrometer. Pulsed field gradient (PFG) NMR self–diffusion measurements were carried out using the PFG–SLED sequence.[32] Dioxane (6% in H_2O, 10 μL) was added to the peptide sample (300 μL) as an internal standard.[31, 54] Pulse lengths and delays in the sequence were held constant and spectra were acquired with the strength of the diffusion gradient varying between 5% and 95% of its maximum value. The pulse gradient width was 4 ms, and the length of the diffusion delay was calibrated for the sample to give a maximal decay of 85–90% for the peptide, peptide/iron or dioxane signals (70, 40 and 18 ms, respectively). Peptide and dioxane NMR spectra were acquired with 4 and 18 K complex points, respectively. The hydrodynamic radius (R_h) was calculated as follows:

$$R_h = (D_{diox}/D_{pep}) \times R_{h,diox} \qquad (1)$$

where Dpep and Ddiox are the measured diffusion coefficients of peptide and dioxane, respectively, and R_h, diox is the effective hydrodynamic radius of dioxane, taken to be 2.12 Å.[31]

Conformational Search and Molecular Dynamics Simulations

To simulate Fe^{3+} metal ions, a set of parameters was fitted performing thermodynamics integrations on MDs (Amber14 [55]) of a metal-water system. The Lennard–Jones parameter for the metal was varied, whereas the charge was set at +3. Ion–oxygen distance and the coordination number were determined by radial distribution function and water residence time analysis.[56]

Possible binding conformations were explored with Autodock4.2 using Lamarckian Genetic Algorithm[57] Conformational search was performed by fixing the backbone to a canonical α-helical conformation. The goal of this search was seeking octahedral coordination geometries for the metal ion. Peptide conformations were clustered into mono–, bi– or tridentate categories according to the number of acid residues involved in metal binding with a distance cutoff of 2.9 Å, and 150 screening cycles (Autodock4.2 parameter *ga_num_eval*) were enough for sampling each cluster.

MDs of free peptide and metal–peptide complexes were carried out using an Amber12 package [55, 58]. Conditions were NPT ensemble, 300 K, time step 2 fs and 15 Å cubic box with TIP3P water molecules. Several 100 ns simulations were performed under an Amber force field ff99SB using PME for long-range electrostatic interactions. Backbone was restricted to the α–helical conformation with a restraint weight of 1.0 kcal mol^{-1} $Å^{-2}$ on $C_α$ atoms. In addition, 500ns MDs without backbone restraints were made for the tridentate complexes using the α-helical conformation as the input structure. Only the last 100 ns of MDs were taken into account for the analysis to minimize bias to the starting conformation.

Notes and references

[a] Instituto de Química y Físico–Química Biológicas, Universidad de Buenos Aires – CONICET. Junín 956, 1113AAD, Buenos Aires, Argentina.
[b] Fundación Instituto Leloir and IIBBA–CONICET, Av. Patricias Argentinas 435, 1405 Buenos Aires, Argentina.

* Correspondence should be addressed to: M.C. González Lebrero at nanolebrero@gmail.com and J. Santos at javiersantosw@gmail.com

‡ These authors contributed equally to this work.

Keywords: Iron binding motif, frataxin, α–helix, peptide grafting, acidic side chains, molecular dynamics simulations.

Abreviations: CD, circular dichroism; CyaY, the frataxin protein family; CZE, capillary zone electrophoresis; Ec–TRX, thioredoxin from *E. coli*; FXN, frataxin protein; GRAP, grafted peptide; ITC, isothermal titration calorimetry; MDs, Molecular Dynamics; PFG, pulsed field gradient; NMR, nuclear magnetic resonance; RMSD, the root–mean–square deviation; SDS, sodium dodecyl sulfate; TFE, 2,2,2–trifluoroethanol; and TRXP, the C–terminal peptide of the thioredoxin protein.

Author Contributions: DSV, NV, AY, MA and FLGF performed experiments and analyzed data. DSV and WAA performed computational experiments and analyzed data. MCGL and JS planned experiments, analyzed data and wrote the paper.

Electronic Supplementary Information (ESI) available: Figure S1. Sequence conservation and AGADIR results. Figure S2, FOLDX results. Figure S3: α–Helical Propensity of GRAP and TRXP; Figure S4: Induction of secondary structure by palladium; Capillary zone electrophoresis results; Figure S5: Capillary Zone Electrophoresis of Peptides; Conformational search using Autodock; Figure S6: Radial functions for water-iron interaction; Table S1: Parameters for Fe^{3+} metal ion simulations using a metal-water system and performing thermodynamic integration on MDs; Table S2: Screening cycle results of

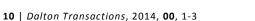*Dalton Transactions Accepted Manuscript*

Autodock evaluation; Figure S7: Side–chain rotamers populated along the MDs. All–atom restrained MDs results; Figures S8 and S9: RMSD analysis of unrestrained MDs; Results on pKa values of the acidic side chains calculated by classical thermodynamic integration; Table S3: Rotamer distribution comparison in MDs; Table S6: The p*K*a values corresponding to each acidic side chain of GRAP calculated by classical thermodynamic integration; References. This material is available free of charge via the Internet at http://pubs.acs.org. See DOI: 10.1039/b000000x/
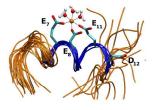
References

1. A. I. Bush, *Curr Opin Chem Biol*, 2000, 4, 184-191.
2. M. Pandolfo and A. Pastore, *J Neurol*, 2009, 256 Suppl 1, 9-17.
3. S. Kono, *Curr Drug Targets*, 2012, 13, 1190-1199.
4. J. R. Connor, S. L. Menzies, J. R. Burdo and P. J. Boyer, *Pediatr Neurol*, 2001, 25, 118-129.
5. K. J. Thompson, S. Shoham and J. R. Connor, *Brain Res Bull*, 2001, 55, 155-164.
6. D. Berg and M. B. Youdim, *Top Magn Reson Imaging*, 2006, 17, 5-17.
7. K. Z. Bencze, K. C. Kondapalli, J. D. Cook, S. McMahon, C. Millan-Pacheco, N. Pastor and T. L. Stemmler, *Crit Rev Biochem Mol Biol*, 2006, 41, 269-291.
8. J. Bridwell-Rabb, A. M. Winn and D. P. Barondeau, *Biochemistry*, 2011, 50, 7265-7274.
9. I. Condo, N. Ventura, F. Malisan, A. Rufini, B. Tomassini and R. Testi, *Hum Mol Genet*, 2007, 16, 1534-1540.
10. S. Dhe-Paganon, R. Shigeta, Y. I. Chi, M. Ristow and S. E. Shoelson, *J Biol Chem*, 2000, 275, 30753-30756.
11. S. Schmucker, M. Argentini, N. Carelle-Calmels, A. Martelli and H. Puccio, *Hum Mol Genet*, 2008, 17, 3521-3531.
12. H. A. Bulteau Al Fau - O'Neill, M. C. O'Neill Ha Fau - Kennedy, M. Kennedy Mc Fau - Ikeda-Saito, G. Ikeda-Saito M Fau - Isaya, L. I. Isaya G Fau - Szweda and L. I. Szweda, *Science* 2004, 305, 242-245.
13. L. E. Gentry, M. A. Thacker, R. Doughty, R. Timkovich and L. S. Busenlehner, *Biochemistry*, 2013, 52, 6085-6096.
14. C. L. Tsai, J. Bridwell-Rabb and D. P. Barondeau, *Biochemistry*, 2011, 50, 6478-6487.
15. T. Bencze Kz Fau - Yoon, C. Yoon T Fau - Millan-Pacheco, P. B. Millan-Pacheco C Fau - Bradley, N. Bradley Pb Fau - Pastor, J. A. Pastor N Fau - Cowan, T. L. Cowan Ja Fau - Stemmler and T. L. Stemmler, *Chem Commun (Camb)*, 2007, 14, 1798-1800.
16. M. Pandolfo, *J Child Neurol*, 2012, 27, 1204-1211.
17. F. Sacca, A. Marsili, G. Puorro, A. Antenora, C. Pane, A. Tessa, P. Scoppettuolo, C. Nesti, V. Brescia Morra, G. De Michele, F. M. Santorelli and A. Filla, *J Neurol*, 2013, 260, 1116-1121.
18. F. Foury, A. Pastore and M. Trincal, *EMBO Rep*, 2007, 8, 194-199.
19. M. Nair, S. Adinolfi, C. Pastore, G. Kelly, P. Temussi and A. Pastore, *Structure*, 2004, 12, 2037-2048.
20. C. Pastore, M. Franzese, F. Sica, P. Temussi and A. Pastore, *FEBS J*, 2007, 274, 4199-4210.
21. A. R. Correia, T. Wang, E. A. Craig and C. M. Gomes, *Biochem J*, 2010, 426, 197-203.
22. A. Binolfi, C. O. Fernandez, M. P. Sica, J. M. Delfino and J. Santos, *Proteins*, 2012, 80, 1448-1464.
23. J. Santos, M. P. Sica, C. M. Buslje, A. M. Garrote, M. R. Ermacora and J. M. Delfino, *Biochemistry*, 2009, 48, 595-607.
24. E. A. Roman, P. Rosi, M. C. Gonzalez Lebrero, R. Wuilloud, F. L. Gonzalez Flecha, J. M. Delfino and J. Santos, *Proteins*, 2010, 78, 2757-2768.
25. S. Adinolfi, M. Trifuoggi, A. S. Politou, S. Martin and A. Pastore, *Hum Mol Genet*, 2002, 11, 1865-1877.
26. W. Humphrey, A. Dalke and K. Schulten, *J Mol Graph*, 1996, 14, 33-38, 27-38.
27. E. Lacroix, A. R. Viguera and L. Serrano, *J Mol Biol*, 1998, 284, 173-191.
28. J. Schymkowitz, J. Borg, F. Stricher, R. Nys, F. Rousseau and L. Serrano, *Nucleic Acids Res*, 2005, 33, W382-388.
29. J. Van Durme, J. Delgado, F. Stricher, L. Serrano, J. Schymkowitz and F. Rousseau, *Bioinformatics*, 2011, 27, 1711-1712.
30. T. Yoon and J. A. Cowan, *J Am Chem Soc*, 2003, 125, 6078-6084.
31. J. Jones, D. Wilkins, L. Smith and C. Dobson, *J Biomol NMR*, 1997, 10, 199-203.
32. M. R. Merrill, *Journal of Magnetic Resonance, Series A*, 1993, 103, 223-225.
33. S. C. Lovell, J. M. Word, J. S. Richardson and D. C. Richardson, *Proteins*, 2000, 40, 389-408.
34. K. Lindorff-Larsen, S. Piana, K. Palmo, P. Maragakis, J. L. Klepeis, R. O. Dror and D. E. Shaw, *Proteins*, 2010, 78, 1950-1958.
35. A. Ortega, D. Amoros and J. Garcia de la Torre, *Biophysical journal*, 2011, 101, 892-898.
36. F. Duarte, P. Bauer, A. Barrozo, B. A. Amrein, M. Purg, J. Aqvist and S. C. Kamerlin, *The journal of physical chemistry. B*, 2014, 118, 4351-4362.
37. F. Gaudreault, M. Chartier and R. Najmanovich, *Bioinformatics*, 2012, 28, i423-i430.
38. G. Kuppuraj, M. Dudev and C. Lim, *The journal of physical chemistry. B*, 2009, 113, 2952-2960.
39. P. F. Predki and B. Sarkar, *J Biol Chem*, 1992, 267, 5842-5846.
40. P. F. Predki and B. Sarkar, *Environmental health perspectives*, 1994, 102 Suppl 3, 195-198.
41. J. Bridwell-Rabb, C. Iannuzzi, A. Pastore and D. P. Barondeau, *Biochemistry*, 2012, 51, 2506-2514.
42. F. Colin, A. Martelli, M. Clemancey, J. M. Latour, S. Gambarelli, L. Zeppieri, C. Birck, A. Page, H. Puccio and S. Ollagnier de Choudens, *J Am Chem Soc*, 2013, 135, 733-740.
43. S. Schmucker, A. Martelli, F. Colin, A. Page, M. Wattenhofer-Donze, L. Reutenauer and H. Puccio, *PLoS One*, 2011, 6, e16199.
44. R. Yan, P. V. Konarev, C. Iannuzzi, S. Adinolfi, B. Roche, G. Kelly, L. Simon, S. R. Martin, B. Py, F. Barras, D. I. Svergun and A. Pastore, *J Biol Chem*, 2013, 288, 24777-24787.
45. F. Bou-Abdallah, S. Adinolfi, A. Pastore, T. M. Laue and N. Dennis Chasteen, *J Mol Biol*, 2004, 341, 605-615.
46. F. Bousejra-ElGarah, C. Bijani, Y. Coppel, P. Faller and C. Hureau, *Inorg Chem*, 2011, 50, 9024-9030.
47. H. M. Fang and Y. Wang, *Biochem J*, 2002, 368, 641-647.
48. D. J. Kosman, *Mol Microbiol*, 2003, 47, 1185-1197.
49. F. Bou-Abdallah, P. Arosio, P. Santambrogio, X. Yang, C. Janus-Chandler and N. D. Chasteen, *Biochemistry*, 2002, 41, 11184-11191.
50. I. Wedderhoff, I. Kursula, M. R. Groves and D. Ortiz de Orue Lucana, *PLoS One*, 2013, 8, e71579.
51. Y. Zhao, J. K. Marzinek, P. J. Bond, L. Chen, Q. Li, A. Mantalaris, E. N. Pistikopoulos, M. G. Noro, L. Han and G. Lian, *Journal of pharmaceutical sciences*, 2014, 103, 1224-1232.
52. Z. Marczenko, *Spectrophotometric determination of elements* Chalmer, R. A. Wiley, New York, 1976.
53. G. E. Crooks, G. Hon, J. M. Chandonia and S. E. Brenner, *Genome Res*, 2004, 14, 1188-1190.
54. D. K. Wilkins, S. B. Grimshaw, V. Receveur, C. M. Dobson, J. A. Jones and L. J. Smith, *Biochemistry*, 1999, 38, 16424-16431.
55. T. A. D. D.A. Case, T.E. Cheatham, III, C.L. Simmerling, J. Wang, R.E. Duke, R. Luo, R.C. Walker, W. Zhang, K.M. Merz, B. Roberts, S. Hayik, A. Roitberg, G. Seabra, J. Swails, A.W. Goetz, I. Kolossváry, K.F. Wong, F. Paesani, J. Vanicek, R.M. Wolf, J. Liu, X. Wu, S.R. Brozell, T. Steinbrecher, H. Gohlke, Q. Cai, X. Ye, J. Wang, M.-J. Hsieh, G. Cui, D.R. Roe, D.H. Mathews, M.G. Seetin, R. Salomon-Ferrer, C. Sagui, V. Babin, T. Luchko, S. Gusarov, A. Kovalenko, and P.A. Kollman, University of California, San Francisco., 12 edn., (2012).
56. H. Ohtaki and T. Radnai, *Chemical Reviews*, 1993, 93, 1157-1204.

57. G. M. Morris, R. Huey, W. Lindstrom, M. F. Sanner, R. K. Belew, D. S. Goodsell and A. J. Olson, *J Comput Chem*, 2009, 30, 2785-2791.
58. R. Salomon-Ferrer, A. W. Götz, D. Poole, S. Le Grand and R. C. Walker, *Journal of chemical theory and computation*, 2013, 9, 3878-3888.

Iron-binding motif **EEXXED** from the first α-helical of frataxin grafted on a foreign peptide scaffold: K_D=1.9±0.2 µM and 1:1 stoichiometry.